

Vibrational phenomena in glasses at low temperatures captured by field theory of disordered harmonic oscillators

Florian Vogel¹ and Matthias Fuchs¹

¹University of Konstanz - D-78457 Konstanz, Germany
(Dated: June 9, 2023)

Abstract- We investigate the vibrational properties of topologically disordered materials by analytically studying particles that harmonically oscillate around random positions. Exploiting classical field theory in the thermodynamic limit at $T = 0$, we build up a self-consistent model by analyzing the Hessian utilizing Euclidean Random Matrix theory. In accordance with earlier findings [T. S. Grigera et al. J. Stat. Mech. 11 (2011) P02015.], we take non-planar diagrams into account to correctly address multiple local scattering events. By doing so, we end up with a first principles theory that can predict the main anomalies of athermal disordered materials, including the boson peak, sound softening, and Rayleigh damping of sound. In the vibrational density of states, the sound modes lead to Debye's law for small frequencies. Additionally, an excess appears in the density of states starting as ω^4 in the low frequency limit, which is attributed to (quasi-) localized modes.

Introduction.— The athermal excitations in glasses differ characteristically from the ones in ordered systems of the same chemical substances. While the vibrational properties of crystalline solids are well understood in terms of phonons, viz. wave-like small particle displacements from lattice positions, the vibrational spectra of amorphous solids exhibit incompletely understood anomalies.

One usually names three phenomena [1]. I) Whereas the Debye law holds in crystalline solids in the low energy regime, there appears a maximum in the reduced vibrational density of states (vDOS) $\frac{g(\omega)}{\omega^2}$ in amorphous solids [1–5]. This maximum is referred to as the *boson peak*, where ω is the frequency. II) Experimental and computational data suggest that the sound attenuation results from disorder-scattering and is Rayleigh-like $\propto \mathbf{p}^4$ below the boson peak, where \mathbf{p} is the wave vector. When entering the frequency regime of the boson peak the damping turns into a \mathbf{p}^2 -law [4, 6–12] which is additionally indicated by a III) softening of the sound velocity, i.e. a dip in the reduced dispersion relation around the frequency of the boson peak [6, 7, 13]. It has been conjectured that these phenomena are interrelated and that they are connected to quasi-localised modes (QLMs) [8, 10, 13–17]. QLMs have been found in many computer simulations of disordered materials. It was also demonstrated that their density of states follows a universal $\propto \omega^4$ law and that they hybridize with phonons, so that neither of the two modes are exact eigenvectors of the dynamical matrix anymore, which is constituted by the Hessian of the potential energy [10, 17, 18].

The localisation of modes in amorphous systems and the resulting fluctuations of elastic constants is at the heart of many prominent models, such as the two-level system [19], the soft potential model [20–22] and its generalizations [23], mean field approaches [5, 24], and the heterogeneous elasticity theory (HET) [8, 13, 16]. Nevertheless, all these approaches require phenomenological parameters and they generally do not capture the vibrational anomalies starting from the microscopic laws of motion. For example, the widely used HET [8, 13, 16]

is a mesoscopic rather than a microscopic theory which quantitatively underestimates the importance of QLMs [14, 15, 25].

In this work, we start from the microscopic equations of disordered coupled harmonic oscillators. This approach leads to the euclidean random matrix (ERM) problem suggested by Parisi and co-workers [2, 26, 27]. Following them, we rely on a Green's function formalism, to derive a self-consistent model that rationalises all aforementioned anomalies and thus improves on earlier ERM-models. The guiding principle in our derivation is that multiple local scattering events are of qualitative importance [28]. This is also hinted at by the discovered influence of non-planar diagrams [29, 30], which were identified as origin of Rayleigh damping in the ERM [31–33]. Therefore, we develop a model that relies on a vertex instead of propagator renormalization.

The system.— We study a system of N particles randomly placed in a volume V at the positions $\{\mathbf{r}_i\}^N$ in the thermodynamic limit with N/V being constant. The positions are drawn from a uniform distribution $P[\{\mathbf{r}_i\}^N] = 1/V^N$. Considering small fluctuations ϕ_i around the frozen positions \mathbf{r}_i , we define the symmetric random matrix \mathbf{M} via the second derivative of an interaction pair potential $U(\{\phi_i\}) = \frac{1}{2} \sum_{i,j=1}^N f(\mathbf{r}_i - \mathbf{r}_j)(\phi_i - \phi_j)^2 = \sum_{i,j} M_{ij} \phi_i \phi_j$. The f is a spring function which quantifies the interaction strength. We only request for the theoretical investigation that the Fourier transformation $\hat{f}(\mathbf{p})$ exists. We also assume rotational invariance, so that \hat{f} only depends on the absolute modulus of the wavevector $p = |\mathbf{p}|$ and that the spring function is regular. This implies $\hat{f}(\mathbf{0}) - \hat{f}(\mathbf{p}) \propto \mathbf{p}^2$ for small \mathbf{p} . When performing numerical calculations, we set $\hat{f}(\mathbf{p}) = (2\pi\sigma^2)^{3/2} e^{-\sigma^2 p^2/2}$. Here σ is an intrinsic length scale of the system, which leads to a dimensionless density $n = N\sigma^3/V$. The density n turns out to be the single state parameter. In the following, σ will be set to unity. Note, that we neglect the vector character of ϕ .

The scalar ϕ_s represent transverse displacements, which predominantly contribute to the boson peak [34].

The fundamental equations of motion of N coupled harmonic oscillators read

$$\ddot{\phi}_i = - \sum_{j=1}^N M_{ij} \phi_j, \quad \text{for } 1 \leq i \leq N. \quad (1)$$

Here, time and (later) frequency are made dimensionless by a frequency scale ω_0 (set to $\omega_0 = 1$ for simplicity) that can be taken from the position of the boson peak in measurements. Translational invariance and hence momentum conservation follow immediately from the potential $U(\{\phi_i\})$. Consequently, \mathbf{M} has the eigenvalue zero. The associated eigenvector \mathbf{e}_0 corresponds to the uniform shift $\mathbf{e}_0 = (1, 1, \dots, 1)$. For positive spring function, the potential U is positive and thus the matrix \mathbf{M} is semi-positive definite.

It is noteworthy, that the disorder in \mathbf{M} and the thermodynamic limit lead to a broadening of the oscillator lines in the dynamic structure factor and to sound attenuation, even though the eigenvalues of the matrix \mathbf{M} are exclusively non-negative and thus the oscillator frequencies real. We interpret this as a instantiation of Landau damping [35]: In time-reversible equations of motion and in the thermodynamic limit, damping can arise from energy transfer among the infinite multitude of modes.

We study the ERM system by analysing the two-point response or Green's function G . It gives the evolution of an initial displacement field with plane wave form of wavevector \mathbf{p} . $G(\mathbf{p}, z)$ is its spectrum at eigenvalue z and is related to the resolvent of \mathbf{M}

$$G(\mathbf{p}, z) = \lim_{N, V \rightarrow \infty} \frac{1}{V} \overline{\sum_{i,j=1}^N e^{i\mathbf{p} \cdot (\mathbf{r}_i - \mathbf{r}_j)} \left[\frac{1}{z - \mathbf{M}} \right]_{ij}}. \quad (2)$$

Here $z = (\omega + i0^+)^2 \in \mathbb{C}$ with ω corresponding to the frequency. The overline indicates the sample average over the disorder. The resolvent can be connected to observables like the dynamic structure factor and the density of states [2, 26, 36]. See the supplemental material (SM), Sect. II [37], for further information.

Self-consistent model.— Following [2, 27, 30], we perform a high density expansion of the resolvent (2). Using the Dyson equation, $G = G_0 + G_0 \Sigma G$, we express the Green's function in terms of a bare propagator $G_0(\mathbf{p}, z) = [z/n - \epsilon_0(\mathbf{p})]^{-1}$ and the self energy $\Sigma(\mathbf{p}, z)$, with $\epsilon_0(\mathbf{p}) = \hat{f}(\mathbf{0}) - \hat{f}(\mathbf{p})$ giving the bare dispersion relation. While G_0 describes undamped harmonic oscillators, Σ arises from the disorder in the elastic couplings. We envision a perturbation traveling through the system, and consider the field ϕ_i as excitation at the respective lattice site so that the interaction between the perturbation and the disorder can be called scattering event [30].

The self energy thus contains all the inelastic scattering events. Σ has a series expansion in $\frac{1}{n}$ and vanishes for $n \rightarrow \infty$, where the disorder vanishes. Thus, $1/n$ quantifies the disorder and the weakening of the elastic constants $f(\mathbf{r}_i - \mathbf{r}_j)$ when the separation of particles gets larger. Using Feynman diagrams, we reconstruct the different inelastic scattering processes. Since this approach has been tried before [2, 27, 30], we moved further comments on the technical details to the SI, Sect. I.

The derivation of our self-consistent model starts with the insight, that any contribution to the self energy necessarily ends with the same vertex and that the momentum is conserved at every vertex. This allows us to write down the self energy schematically:

$$\Sigma(\mathbf{p}, z) = \text{Diagram 1} \quad (3)$$

$$\text{Diagram 1} = \text{Diagram 2} + \text{Diagram 3} + \text{Diagram 4} + \dots$$

Here, a straight line represents the bare propagator; a curly line a density fluctuation and the circle denotes a vertex and marks an inelastic scattering event. The square can be regarded as a renormalized vertex [38], which absorbs all possible insertions at a bare vertex. The letters A, B, C just label the different building blocks in (3) which are of second order in density fluctuation. The three dots represent more diagrams with more simultaneous density fluctuations. Every new loop comes with an additional factor $1/n$. Thus, one can truncate the expansion after a few orders in the high density limit.

A self-consistent model is easily constructed by only keeping classes of diagrams with the topologies A, B , and C and, in the lower line of Eq. (3), by replacing the bare propagator between two bare vertices with the full Green's function $G(\mathbf{p}, z)$. (Note, a dressed Green's function ending in a renormalized vertex would lead to an overcounting. This can be easily seen by inserting the Dyson equation.) In contrast to earlier models [2, 33, 39], this re-summation takes all the diagrams that topologically match the ones from second order perturbation theory and hence non-planar diagrams into account. We do this for two related reasons: I) QLMs are arguably important for the modes of vibrations of low temperature glasses [14, 15, 17, 40] and one must therefore correctly consider multiple local scattering events. Planar diagrams underestimate these scattering sequences [14, 15, 28]. II) Non-planar diagrams are needed to give the correct Rayleigh-damping of sound modes for $p \rightarrow 0$ and to prevent a potential infrared divergence of the self energy [29, 41]. The Feynman rules stated in the SI, Sect. I, allow to write down the associated amplitude for

our self-consistent model

$$G(\mathbf{p}, z) = \frac{1}{z/n - \epsilon_0(\mathbf{p}) - \Sigma(\mathbf{p}, z)}, \quad (4a)$$

$$\Sigma(\mathbf{p}, z) = \int \frac{d^3 \mathbf{k}}{(2\pi)^3} V(\mathbf{k}, \mathbf{p}) \mathcal{V}(\mathbf{k}, \mathbf{p}, z), \quad (4b)$$

$$\begin{aligned} & \left[nG_0^{-1}(\mathbf{k}, z) - \int \frac{d^3 \mathbf{q}}{(2\pi)^3} V^2(\mathbf{q}, \mathbf{k}) G(\mathbf{q}, z) \right] \mathcal{V}(\mathbf{k}, \mathbf{p}, z) \\ &= V(\mathbf{k}, \mathbf{p}) + \int \frac{d^3 \mathbf{q}}{(2\pi)^3} \left[V(\mathbf{q} - \mathbf{k}, 2\mathbf{q} - \mathbf{p}) + V(\mathbf{p} - \mathbf{q}, \mathbf{k}) \right. \\ & \quad \left. \times G(|\mathbf{p} - \mathbf{k} - \mathbf{q}|, z) V(\mathbf{p} - \mathbf{k}, \mathbf{q}) \right] \mathcal{V}(\mathbf{q}, \mathbf{p}, z), \quad (4c) \end{aligned}$$

$$V(\mathbf{k}, \mathbf{p}) = \hat{f}(\mathbf{k}) - \hat{f}(\mathbf{k} - \mathbf{p}) = -V(\mathbf{p} - \mathbf{k}, \mathbf{p}). \quad (4d)$$

While one could easily include more diagrams, there is no need for it. On the contrary, we will now argue that this minimal model successfully captures all the vibrational phenomena of low temperature glasses. Importantly, we consider stable glass states while previous approaches had considered marginally stable glasses where a close-by instability leads to vibrational anomalies [2, 39, 42].

Results.– a) Dispersion relation: The dispersion relation $\epsilon(\mathbf{p}) = n(\epsilon_0(\mathbf{p}) + \text{Re}[\Sigma(\mathbf{p}, z = 0)])$ characterizes the peak positions of the vibrational modes in the dynamic structure factor; it is shown in Fig. 1. The limiting proportionality $\epsilon(p) \propto n$ for $n \rightarrow \infty$ arises from the pairwise interaction among all particles. The expansion $\epsilon(\mathbf{p} \rightarrow 0) \rightarrow (c_T p)^2$ indicates the presence of sound waves in the hydrodynamic limit. They are expected as Goldstone modes arising from broken translational invariance. Here, c_T is the (transverse) speed of sound. Lowering the density increases the disorder and weakens the elasticity; the frequencies of vibrations become softer. Additionally, a dip appears around $\sigma p \approx 10$. This indicates a negative dispersion of the sound velocity, *i.e.* sound softening, and also suggests the presence of the boson peak in the vDOS [6, 7, 13]. For very small n , $\epsilon(p \approx 10/\sigma)$ may become negative, but this density range is not considered. Considering only diagrams of type *A* in Eq. (3), a self-consistent re-summation of all planar diagrams is possible [2, 39], which for reference is presented in the SI, Sect. V. It captures wave modes equally well and gives comparable results for $\epsilon(p)$ as included in Fig. 1.

b) Sound attenuation: The sound attenuation is given by the imaginary part of the self-energy. It determines the width of the vibrational mode around the sound pole. The self-consistent re-summation of the planar diagrams alone [2, 30, 39] leads to strong hydrodynamic sound damping (*viz.* $\propto p^2$), while experiments [6, 12] and simulations [7, 14, 43] indicate weaker Rayleigh damping (*viz.* $\propto p^4$). It can be understood to result from wave scattering off the frozen disorder. To show that the non-planar diagrams fix the error of a planar self-consistent approach, we argue that the imaginary parts

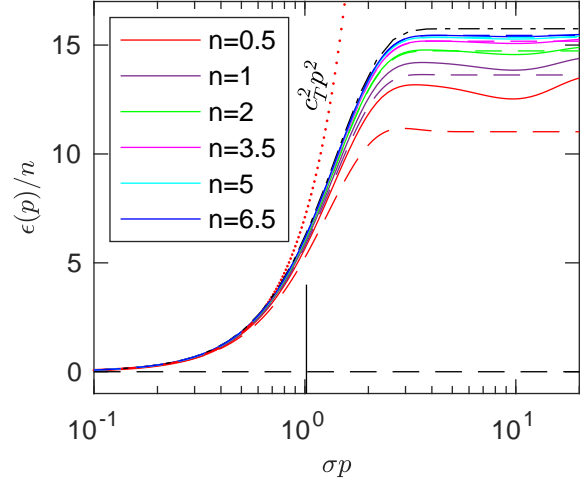
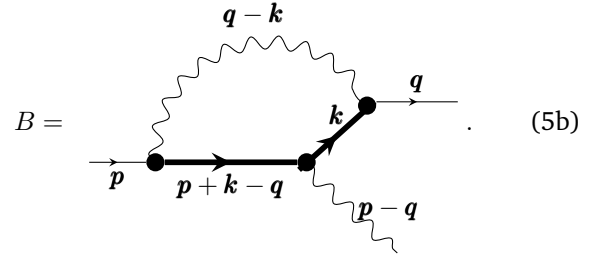
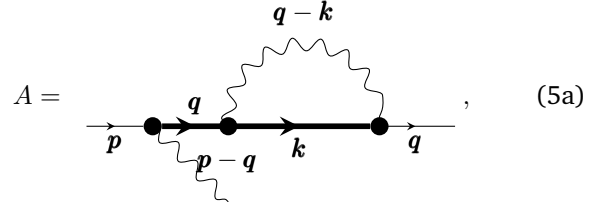


Figure 1. The reduced dispersion relation $\epsilon(p)/n$ (solid lines) is shown for different densities as function of wavevector p . It is compared to the associated bare dispersion $\epsilon_0(p)$ (dashed-dotted line) and to the result from the planar re-summation (dashed lines) [39]. The limit of sound propagation, $\epsilon(p \rightarrow 0) \rightarrow (c_T p)^2$ is indicated for $n = 0.5$. At this n , the vertical bar marks $p_{BP} = \omega_{BP}/c_T$, the wavenumber delimiting the sound behavior.

of the planar diagrams (class *A*, first line in Eq. (4c) and given in diagram (5a)) and non-planar diagrams (class *B*, last line in Eq. (4c) and given in diagram (5b)) cancel each other exactly for $\mathbf{p} \rightarrow 0$.



The thick line represents the full Green's function. Both diagrams describe equivalent scattering processes off two density fluctuations but in different sequence. The cancellation can be seen by applying the Sokhotski-Plemelj identity $[x \pm i0^\pm]^{-1} = \mp i\pi\delta(x) + \mathcal{P}(\frac{1}{x})$ to the full propagator in the hydrodynamic limit and by integrating over \mathbf{k} ; here, \mathcal{P} represents the Cauchy-principal value. For small \mathbf{p} , the symmetry (4d) gives the cancel-

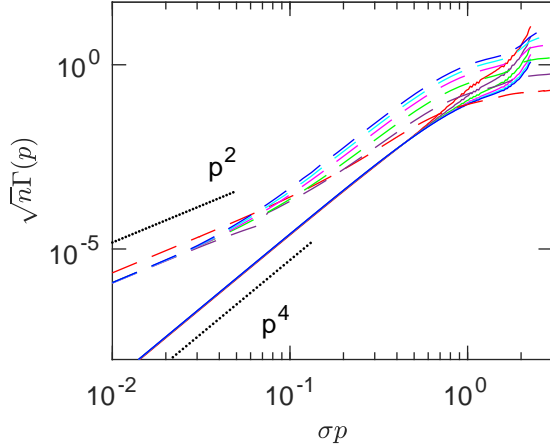


Figure 2. Sound attenuation as function of wavevector p . Rescaled data $\sqrt{n}\Gamma(p)$ collapse for high densities n (see legend in Fig. 1) for small p . Solid lines follow from the imaginary part of the self-energy given by Eq. (4), dashed lines follow from planar diagrams [39] (see SI). The sound attenuation is calculated around the sound pole $\omega = \sqrt{n\epsilon_0(p)}$. Dotted lines represent asymptotic power laws.

lation; see proof in the SI, Sect. III. It also fixes the infrared divergence problem [29, 41]. The building block containing the four vertex (diagram C in (S5) in the SI) gives the correct imaginary part by itself. In total, this leads to $G(\mathbf{p}, z)/n = [z - \epsilon(\mathbf{p}) - i\omega(\mathbf{p})\Gamma(\mathbf{p})]^{-1}$ with $\Gamma(\mathbf{p}) = n\text{Im}\Sigma(\mathbf{p}, z = \epsilon(\mathbf{p}))/\omega(\mathbf{p}) = B_R p^4$ around the sound pole $\omega(\mathbf{p}) = \sqrt{\epsilon(\mathbf{p})}$ in the hydrodynamic limit. The strength of Rayleigh damping B_R increases with disorder.

Figure 2 shows the sound attenuation for different densities in the two loop approximation; see the SI for details. Since our full model (4) topologically coincides with the second order, the second order solution confirms, that (4) predicts the correct sound attenuation.

c) Vibrational density of states: The vDOS can be calculated from the large wavevector limit of the Green's function where only diagonal elements of \mathbf{M} contribute in Eq. (2) [2, 27]; see SI, Sect. IV, for details. The sound modes already identified in the dispersion relation suggest that the vDOS contains a Debye spectrum $g_D(\omega) = \omega^2/\omega_D^3$ for $\omega \rightarrow 0$. The Debye frequency ω_D characterizes the region of long-wavelength sound and gives an upper cut-off for waves in solids. It shrinks with increasing disorder and the magnitude of the Debye law increases for decreasing n ; see panel a) in Fig. 3. Note, that panel a) has been calculated under the assumption that ω^2 is small; see SI, Sect. IV. This approximation breaks down for $\omega \rightarrow 1$. The boson peak is situated at the upper end of the spectrum of vibrations in the model. There, the vDOS can be simplified as the contributions of the acoustic phonons to the self energy become weak. This leads to a closed expression for the vDOS which is

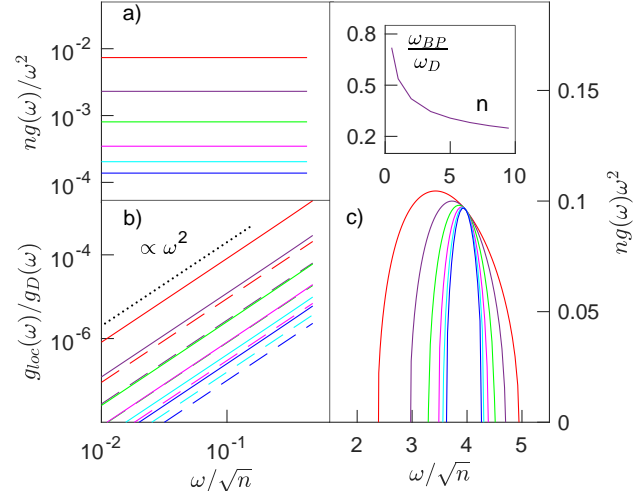


Figure 3. Panel a), full lines show the reduced vibrational density of states (vDOS), $ng(\omega)/\omega^2$, for low frequencies at different number densities n . Panel b) presents the vDOS of the quasi-localised modes (QLM), $g_{loc}(\omega)/g_D(\omega)$, where the dashed line shows the prediction of the HET theory. Panel c) exhibits the rescaled boson peak, $ng(\omega)/\omega^2$, which is located at the upper end of the dispersion relation. The inset shows the ratio ω_{BP}/ω_D of boson peak and Debye frequencies. The densities and their respective colours are the same in all three panels following the legend in Fig. 1.

Wigner's semi circle law as expected in uncorrelated random matrix ensembles [5, 36, 44]. The amplitude of the boson peak shown in panel c) of Fig. 3 only varies little with increasing disorder, while its position shifts trivially with \sqrt{n} . The ratio of its position to the Debye-frequency, ω_{BP}/ω_D (see the inset in panel c) of Fig. 3), is smaller as one indicating that ω_{BP} , and not ω_D , sets the limit for wave behavior in random matrix approaches [13, 45]. In simulations of stable glasses [46], the boson peak lies low, $\omega_{BP}/\omega_D \approx 0.17$.

d) Quasi localised modes: Recent works [8, 14, 17, 46] established a close relation between QLMs and Rayleigh-damping by showing that there is a linear relation between the damping coefficient B_R and the coefficient A_4 of the characteristic vDOS of the quasi localised modes $g_{loc} = A_4\omega^4$. Additionally, it was argued in [47] that the presence of QLMs implies a p^4 sound attenuation. Furthermore, it has been shown that QLMs give rise to the boson peak [1, 10, 14, 17, 22]. This suggests that QLMs are at the heart of the vibrational anomalies of disordered materials. Our results in Figs. 2 and 3 support this narrative. In finite systems, the participation ratio can be used to identify QLMs, which is impossible here as the thermodynamic limit was taken. Thus, we interpret the QLMs as the modes that have a vDOS proportional to the Rayleigh term B_R . We show the quartic contribution to the vDOS in panel b) of Fig. 3, again utilising a small ω approximation. We also compare it to the HET-prediction $g_{loc}^{HET}/\omega^4 = 2B_R/(\pi\omega_D^2 c_T^4)$

[8, 10], which underestimates disorder in stable glasses quantitatively [14, 46], where $(c_T^4 \omega_{BP}^2) A_4 / B_R \approx 0.05$ holds; our ratio 0.045 for $n = 0.5$ lies close. The anomaly is missing in the vDOS of the self-consistent planar theory [2, 39], which confirms that planar diagrams overly restrict the sequence of interactions of vibrational modes with particle sites; for details see the SI, Sect. V.

Conclusion and Outlook.— Our self-consistent field theory of ERM accounts for disorder more accurately than approaches based on mean field or coherent potential approximations. The latter underestimate multiple local scattering events, which become important if one has bound states or localisation effects [28]. Neglecting dependent scattering processes in an ERM model leads to a planar theory for the vDOS in the thermodynamic limit [36]. This, together with the cancellation of diagrams in Eq. (5) to get the correct Rayleigh damping suggests that non-planar diagrams are essential to correctly address disorder. Besides this qualitative insight, we constructed a self consistent theory for disordered harmonic oscillators that correctly predicts all the vibrational anomalies of disordered materials. It can be coarse-grained and then leads to the widely-used HET. After understanding the topology of athermal disorder, the next step is to take the vector character of the displacement fields into account and to consider finite temperatures. Additionally, it would be worthwhile to relate the approach to the soft potential model and its generalizations.

Acknowledgment.— We thank Matthias Krüger for the co-supervision of the Master’s thesis that was the basis for this work, and him, Annette Zippelius, Thomas Franosch, and Walter Schirmacher for fruitful discussions. The work was supported by the Deutsche Forschungsgemeinschaft (DFG) via SFB 1432 project CO7.

REFERENCES

- [1] A. Marruzzo, S. Köhler, A. Fratolocci, G. Ruocco, and W. Schirmacher. Vibrational anomalies and marginal stability of glasses. *The European Physical Journal Special Topics*, 216(1), 2013.
- [2] S. Ciliberti, TS. Grigera, V. Martin-Mayor, G. Parisi, and P. Verrocchio. Brillouin and boson peaks in glasses from vector euclidean random matrix theory. *The Journal of chemical physics*, 119(16):8577–8591, 2003.
- [3] J. Wuttke, W. Petry, G. Coddens, and F. Fujara. Fast dynamics of glass-forming glycerol. *Phys. Rev. E*, 52:4026–4034, Oct 1995.
- [4] G. Baldi, V. M. Giordano, G. Monaco, and B. Ruta. Sound attenuation at terahertz frequencies and the boson peak of vitreous silica. *Phys. Rev. Lett.*, 104:195501, May 2010.
- [5] S. Franz, G. Parisi, P. Urbani, and F. Zamponi. Universal spectrum of normal modes in low-temperature glasses. *Proc. Nat. Acad. Sci.*, 112(47):14539–14544, 2015.
- [6] G. Monaco and V. Giordano. Breakdown of the debye approximation for the acoustic modes with nanometric wavelengths in glasses. *Proceedings of the National Academy of Sciences*, 106(10):3659–3663, 2009.
- [7] G. Monaco and S. Mossa. Anomalous properties of the acoustic excitations in glasses on the mesoscopic length scale. *Proceedings of the National Academy of Sciences*, 106(40):16907–16912, 2009.
- [8] W. Schirmacher, G. Ruocco, and T. Scopigno. Acoustic attenuation in glasses and its relation with the boson peak. *Phys. Rev. Lett.*, 98:025501, Jan 2007.
- [9] A. Marruzzo, W. Schirmacher, A. Fratolocci, and G. Ruocco. Heterogeneous shear elasticity of glasses: the origin of the boson peak. *Scientific Reports*, 3(1):1407, 2013.
- [10] H. Mizuno and A. Ikeda. Phonon transport and vibrational excitations in amorphous solids. *Phys. Rev. E*, 98:062612, 2018.
- [11] G. Baldi, V. M. Giordano, B. Ruta, R. Dal Maschio, A. Fontana, and G. Monaco. Anharmonic damping of terahertz acoustic waves in a network glass and its effect on the density of vibrational states. *Phys. Rev. Lett.*, 112:125502, Mar 2014.
- [12] G. Baldi, M. Zanatta, E. Gilioli, V. Milman, K. Refson, B. Wehinger, B. Winkler, A. Fontana, and G. Monaco. Emergence of crystal-like atomic dynamics in glasses at the nanometer scale. *Phys. Rev. Lett.*, 110:185503, 2013.
- [13] W. Schirmacher and G. Ruocco. Heterogeneous elasticity: The tale of the boson peak; arxiv:2009.05970, 2020.
- [14] L. Wang, L. Berthier, E. Flenner, P. Guan, and G. Szamel. Sound attenuation in stable glasses. *Soft Matter*, 15:7018–7025, 2019.
- [15] G. Szamel and E. Flenner. Microscopic analysis of sound attenuation in low-temperature amorphous solids reveals quantitative importance of non-affine effects. *The Journal of Chemical Physics*, 156(14):144502, apr 2022.
- [16] S. Mahajan and M. P. Ciamarra. Unifying description of the vibrational anomalies of amorphous materials. *Physical Review Letters*, 127(21):215504, nov 2021.
- [17] E. Lerner and E. Bouchbinder. Low-energy quasilocalized excitations in structural glasses. *The Journal of Chemical Physics*, 155(20):200901, nov 2021.
- [18] D. Richard, K. González-López, G. Kapteijns, R. Pater, T. Vaknin, E. Bouchbinder, and E. Lerner. Universality of the nonphononic vibrational spectrum across different classes of computer glasses. *Phys. Rev. Lett.*, 125:085502, Aug 2020.
- [19] P. W. Anderson, B. I. Halperin, and C. M. Varma. Anomalous low-temperature thermal properties of glasses and spin glasses. *The Philosophical Magazine: A Journal of Theoretical Experimental and Applied Physics*, 25(1):1–9, 1972.
- [20] Yu.M. Galperin, V.G. Karpov, and V.I. Kozub. Localized states in glasses. *Advances in Physics*, 38(6):669–737, 1989.
- [21] D. A. Parshin. Soft potential model and universal properties of glasses. *Physica Scripta*, T49A:180–185, jan 1993.
- [22] D. A. Parshin, H. Schober, and Yu. M. Gurevich. Vibrational instability, two-level systems, and the boson peak in glasses. *Physical Review B*, 76(6):064206, aug 2007.
- [23] E. Bouchbinder, E. Lerner, C. Rainone, P. Urbani, and F. Zamponi. Low-frequency vibrational spectrum of mean-field disordered systems. *Phys. Rev. B*, 103:174202, May 2021.
- [24] E. DeGiuli, A. Laversanne-Finot, G. Düring, E. Lerner,

- and M. Wyart. Effects of coordination and pressure on sound attenuation, boson peak and elasticity in amorphous solids. *Soft Matter*, 10:5628–5644, 2014.
- [25] C. Caroli and A. Lemaître. Fluctuating elasticity fails to capture anomalous sound scattering in amorphous solids. *Phys. Rev. Lett.*, 123:055501, Jul 2019.
- [26] M. Mézard, G. Parisi, and A. Zee. Spectra of euclidean random matrices. *Nuclear Physics B*, 559(3):689–701, 1999.
- [27] V. Martin-Mayor, M. Mézard, G. Parisi, and P. Verrocchio. The dynamical structure factor in topologically disordered systems. *The Journal of Chemical Physics*, 114(18):8068–8081, 2001.
- [28] P. Sheng. *Introduction to Wave Scattering, Localization, and Mesoscopic Phenomena*. Elsevier Science, 1995.
- [29] E. Leutheusser. Self-consistent kinetic theory for the lorentz gas. *Phys. Rev. A*, 28:1762–1773, 1983.
- [30] T. S. Grigera, V. Martin-Mayor, G. Parisi, P. Urbani, and P. Verrocchio. On the high-density expansion for euclidean random matrices. *Journal of Statistical Mechanics: Theory and Experiment*, 2011(02):P02015, 2011.
- [31] C. Ganter and W. Schirmacher. Rayleigh scattering, long-time tails, and the harmonic spectrum of topologically disordered systems. *Phys. Rev. B*, 82:094205, 2010.
- [32] C. Ganter and W. Schirmacher. Euclidean random matrix theory: low-frequency non-analyticities and rayleigh scattering. *Phil. Mag.*, 91(13-15):1894–1909, 2011.
- [33] W. Schirmacher, V. Folli, C. Ganter, and G. Ruocco. Self-consistent euclidean-random-matrix theory. *J. Phys. A: Math. Theo.*, 52(46):464002, 2019.
- [34] J. Horbach, W. Kob, and K. Binder. High frequency sound and the boson peak in amorphous silica. *The European Physical Journal B-Condensed Matter and Complex Systems*, 19:531–543, 2001.
- [35] C. Mouhot and C. Villani. On landau damping. *Acta mathematica*, 207(1):29–201, 2011.
- [36] A. Goetschy and S. E. Skipetrov. Euclidean random matrices and their applications in physics, arXiv1303.2880 (2013).
- [37] See Supplemental Material at <http://> for additional details on Feynman rules, analytical calculations, and a comparison with the planar theory.
- [38] A.K. Chattopadhyay, A. Basu, and J. K. Bhattacharjee. Coupled nonequilibrium growth equations: Self-consistent mode coupling using vertex renormalization. *Physical Review E*, 61(2):2086, 2000.
- [39] T. S. Grigera, V. Martín-Mayor, G. Parisi, and P. Verrocchio. Vibrational spectrum of topologically disordered systems. *Phys. Rev. Lett.*, 87:085502, Aug 2001.
- [40] H. R. Schober and G. Ruocco. Size effects and quasilocalized vibrations. *Philosophical Magazine*, 84(13-16):1361–1372, 2004.
- [41] S. Schnyder, F. Höfling, T. Franosch, and Th. Voigtmann. Long-wavelength anomalies in the asymptotic behavior of mode-coupling theory. *Journal of Physics: Condensed Matter*, 23(23):234121, 2011.
- [42] M. Shimada, H. Mizuno, and A. Ikeda. Vibrational spectrum derived from local mechanical response in disordered solids. *Soft Matter*, 16(31):7279–7288, 2020.
- [43] H. Mizuno, H. Shiba, and A. Ikeda. Continuum limit of the vibrational properties of amorphous solids. *Proceedings of the National Academy of Sciences*, 114(46):E9767–E9774, 2017.
- [44] W. Götze and M. R. Mayr. Evolution of vibrational excitations in glassy systems. *Phys. Rev. E*, 61:587–606, 2000.
- [45] D. A. Conyuh and Y. M. Beltukov. Random matrix approach to the boson peak and ioffe-regel criterion in amorphous solids. *Phys. Rev. B*, 103:104204, Mar 2021.
- [46] L. Wang, A. Ninarello, P. Guan, L. Berthier, G. Szamel, and E. Flenner. Low-frequency vibrational modes of stable glasses. *Nature Communications*, 10(1), 2019.
- [47] H.R. Schober. Quasi-localized vibrations and phonon damping in glasses. *Journal of Non-Crystalline Solids*, 357(2):501–505, 2011. 6th International Discussion Meeting on Relaxation in Complex Systems.
- [48] P. Coleman. *Introduction to Many-Body Physics*. Cambridge Press, 2015.

Supplemental Materials for "Vibrational phenomena in glasses at low temperatures captured by field theory of disordered harmonic oscillators"

Florian Vogel¹ and Matthias Fuchs¹

¹University of Konstanz - D-78457 Konstanz, Germany

(Dated: June 9, 2023)

I. FEYNMAN RULES

The main focus in this paper lies on the averaged Green's function, which is the Fourier and Laplace transformed two-point response function with $-s^2 = z$, where $s = -i\omega + 0^+$ is the Laplace frequency

$$G(\mathbf{p}, z) = -\frac{1}{V} \frac{1}{s} \sum_{i,j=1}^N \int d^3\mathbf{r}_i d^3\mathbf{r}_j P_2(\mathbf{r}_i, \mathbf{r}_j) \int_0^\infty e^{-i\mathbf{q}\cdot(\mathbf{r}_j-\mathbf{r}_i)} e^{-st} \langle \phi(\mathbf{r}_i, t), \phi(\mathbf{r}_j, 0) \rangle, \quad (\text{S1})$$

with $\text{Re}[z] > 0$ and $\phi(\mathbf{r}_i, t)$ being the elongation of the i^{th} particle from its equilibrium position. $\langle \cdot \cdot \cdot \rangle$ representing the average in a given quenched disorder. Since we consider zero temperature, the average in the quenched disorder can be pictured as sending a sound mode through the same configuration of particles with different starting positions and then taking the average of the different two-point functions. The integrals over the positions $\{\mathbf{r}_i\}^N$ give the average over the disorder. Here, $P_2(\mathbf{r}_i, \mathbf{r}_j)$ is the joint probability distribution of the particle locations. In this paper, we assume uniform and independent distributions $P_2(\mathbf{r}_i, \mathbf{r}_j) = P_1(\mathbf{r}_i)P_1(\mathbf{r}_j) = 1/V^2$.

Unfortunately, one can only calculate the two-point function analytically in exceptional cases. Hence, one relates the interacting system to the non-interacting system using the Gell-Mann Low theorem [48]. Assuming that the interaction is weak and turned on adiabatically, one can describe the full system as a perturbation of the non-interactive system. The resolvent of the latter, the bare propagator is denoted by G_0 . The interaction can be interpreted as inelastic scattering events of a vibrational wave with the disorder that causes density fluctuations. The associated Feynman rules have been lucidly derived in [30] using a field theoretical and a combinatorial approach. Thus, we just state the Feynman rules and refer to the cited paper for the derivation.

• Field Excitation:  $= G_0(\mathbf{p}, z) = \frac{1}{z/n - \epsilon_0(\mathbf{p})}$ (S2a)

• Density Fluctuation:  $= 1$ (S2b)

• Three Vertex:  $= V(\mathbf{q}, \mathbf{p}) = \hat{f}(\mathbf{q}) - \hat{f}(\mathbf{q} - \mathbf{p})$ (S2c)

• Four Vertex:  $= V(\mathbf{q} - \mathbf{k}, 2\mathbf{q} - \mathbf{p})$ (S2d)

Note, that we use a slightly different notation compared to [2, 30]. We pulled out the density to make the dependence on this parameter more transparent. While the bare propagator only considers stiff connections between the particles, the full Green's function also takes scattering processes into account. The difference between the two propagators is the self-energy $\Sigma(\mathbf{p}, z) = G_0^{-1}(\mathbf{p}, z) - G^{-1}(\mathbf{p}, z)$, which hence encodes the full complexity of the system.

II. OBSERVABLES

The two observables considered in this work are the dynamic structure factor S_λ and the vibrational density of states g_λ . Both can be related to the Green's function. S_λ measures the correlation between the position of the i^{th} particle at time 0 and the j^{th} particle at time t . The subscripted λ refers to the eigenvalue space, in which the dynamic structure factor reads

$$\begin{aligned} S_\lambda(\mathbf{p}, \lambda) &= \lim_{N \rightarrow \infty} \frac{1}{2N} \sum_n \sum_{i,j=1}^N \overline{e^{i\mathbf{p} \cdot (\mathbf{r}_j - \mathbf{r}_i)} e_n(i) e_n(j) \delta(\lambda - \lambda_n)} \\ &= -\frac{1}{n\pi} \text{Im}G(\mathbf{p}, \lambda + i0^+). \end{aligned} \quad (\text{S3})$$

Here, the overline denotes the average for an arbitrary but fixed disorder, $\lambda = \omega^2 = z$ represents the energy values and λ_n are the eigenvalues of \mathbf{M} . The Hessian matrix is determined by the spring function, $M_{ij} = \delta_{ij} \sum_k f(\mathbf{r}_i - \mathbf{r}_k) - f(\mathbf{r}_i - \mathbf{r}_j)$. The dynamic structure factor exhibits peaks around the sound poles $z = n(\epsilon_0(\mathbf{p}) + \text{Re}\Sigma(\mathbf{p}, z))$ with the self energy Σ introduced in Eq. (4a). The width of these peaks is given by the imaginary part of the self energy, which hence determines the sound attenuation.

The density of states is given by the trace of the resolvent and thus by the high momentum limit of the dynamic structure factor [2, 27, 30]. This gives the expression

$$g_\lambda(\lambda) \equiv \frac{1}{N} \sum_n \delta(\lambda - \lambda_n) = -\frac{1}{n\pi} \lim_{p \rightarrow \infty} \text{Im}G(p, \lambda + i0^+). \quad (\text{S4})$$

The density of states in the frequency domain is obtained by multiplying $g_\lambda(\lambda)$ with the Jacobian $|\frac{\partial \lambda}{\partial \omega}|$. This gives $g(\omega) = 2\omega g_\lambda(\lambda(\omega))$.

III. RAYLEIGH DAMPING OF THE SELF-CONSISTENT MODEL

It has already been proven in [30] that the Euclidean random matrix model without any approximations predicts Rayleigh-damping. In this section, we prove that our self consistent model (4) does so as well. The idea is that the imaginary part of the self-energy in the lowest order arises from the imaginary part of exactly one of the propagators constituting a diagram times the real part of the remaining ones.

Considering an arbitrary diagram it is self-evident from (4) that every diagram from second order onwards can be built up from the following three building blocks plus an initial and a final vertex $V(\mathbf{q}', \mathbf{p})$ or respectively $V(\mathbf{k}', \mathbf{p})$

$$A = \quad B = \quad C = \quad (\text{S5})$$

The crucial point is, that the imaginary part of the A - and B -blocks cancel each other out exactly. As a consequence, the lowest surviving order of the imaginary part of the self energy is Rayleigh-like $\text{Im}\Sigma \propto \sqrt{\lambda} p^4$. To make the building-block structure appear in the equation for the renormalised vertex, we pull out a factor $G_0^{-1}(\mathbf{k}, z)$ from the

renormalised vertex $\mathcal{V}(\mathbf{k}, \mathbf{p}, z) \rightarrow G_0^{-1}(\mathbf{k}, z)\mathcal{V}(\mathbf{k}, \mathbf{p}, z)$. The self-consistent equations for the self energy hence read

$$\begin{aligned}\Sigma(\mathbf{p}, z) &= \sum_{\mathbf{k}} V(\mathbf{k}, \mathbf{p}) G_0(\mathbf{k}, z) \mathcal{V}(\mathbf{k}, \mathbf{p}, z), \\ \mathcal{V}(\mathbf{k}, \mathbf{p}, z) &= \frac{V(\mathbf{k}, \mathbf{p})}{n} + \frac{1}{n} \sum_{\mathbf{q}} \left\{ \sum_{\mathbf{l}} V^2(\mathbf{l}, \mathbf{k}) G(\mathbf{l}, z) \delta(\mathbf{k} - \mathbf{q}) \right. \\ &\quad \left. + V(\mathbf{q} - \mathbf{k}, 2\mathbf{q} - \mathbf{p}) + V(\mathbf{p} - \mathbf{q}, \mathbf{k}) G(\mathbf{p} - \mathbf{q} - \mathbf{k}, z) V(\mathbf{p} - \mathbf{k}, \mathbf{q}) \right\} G_0(\mathbf{q}, z) \mathcal{V}(\mathbf{q}, \mathbf{p}, z),\end{aligned}\quad (\text{S6})$$

with $\sum_{\mathbf{k}} = \int \frac{d\mathbf{k}}{(2\pi)^3}$. For simplicity of notation, integrals over wavevectors are abbreviated as summations throughout the supplemental information. We will now analyse this equation term by term by applying the Sokhotski-Plemelj formula

$$\frac{1}{x + i0^+} = P \frac{1}{x} - i\pi \delta(x), \quad (\text{S7})$$

with P denoting the Cauchy Principal value.

1.) The first term leads to the first order perturbation theory

$$\frac{1}{n} \sum_{\mathbf{k}} V(\mathbf{k}, \mathbf{p}) G_0(\mathbf{k}, \lambda + i0^+) \mathcal{V}(\mathbf{k}, \mathbf{p}, \lambda + i0)^{(1)} = -\frac{1}{n} \sum_{\mathbf{k}} V(\mathbf{k}, \mathbf{p}) G_0(\mathbf{k}, \lambda + i0^+) V(\mathbf{k}, \mathbf{p}) \quad (\text{S8})$$

Applying (S7) gives the correct order of eigenvalue and momentum in the hydrodynamic limit, *i.e.* $\text{Im}\Sigma^{(1)} = a\lambda^{\frac{1}{2}}p^4 + b\lambda^{\frac{3}{2}}p^2$, with $a, b \in \mathbb{R}$. The notation $\mathcal{V}^{(m)}$ denotes the m^{th} term in equation (S6).

2.) The next term is more complicated since the renormalised vertex \mathcal{V} appears left and right of the equality sign. But again, the imaginary part results from a single loop in the hydrodynamic limit. Everything else would lead to higher orders in λ since the imaginary part of any loop vanishes with the eigenvalue. Hence, one can look at a single term/loop in \mathcal{V} . By doing so, one leaves it open what might appear to the left or right of it. Applying (S7) yields

$$\text{Im}\mathcal{V}(\mathbf{k}, \mathbf{p}, \lambda + i0^+)^{(2)} = \frac{1}{n} \sum_{\mathbf{q}} V(\mathbf{q} - \mathbf{k}, 2\mathbf{q} - \mathbf{p}) \text{Im}G_0(\mathbf{q}, \lambda + i0^*) \mathcal{V}(\mathbf{q}, \mathbf{p}, \lambda) \quad (\text{S9})$$

$$\xrightarrow{\lambda \rightarrow 0} -\frac{\pi S_3}{2(2\pi)^3 c_0^2} \left(\frac{\lambda}{c_0^2} \right)^{\frac{1}{2}} V(\mathbf{k}, \mathbf{p}) \mathcal{V}(0, \mathbf{p}, \lambda) \propto \lambda^{\frac{1}{2}} \mathbf{p} \mathcal{V}(0, \mathbf{p}, \lambda), \quad (\text{S10})$$

with the speed of sound $c_0 = \lim_{q \rightarrow 0} \frac{\sqrt{n\epsilon_0(\mathbf{q})}}{q}$ of the bare system and S_3 being the surface area of the unit sphere.

Since the initial and final two vertices both give an additional factor \mathbf{p} , the contribution to the imaginary part of the self-energy arising from the imaginary part of $\mathcal{V}^{(2)}$ is at least of order $\lambda^{\frac{1}{2}}\mathbf{p}^3$. But such a term can not appear due to momentum inversion invariance. So the leading order must be at least $\lambda^{\frac{1}{2}}\mathbf{p}^4$.

Note that one could also apply (S7) to the bare propagator $G_0(\mathbf{k}, z)$ in

$$\frac{1}{n} \sum_{\mathbf{k}, \mathbf{q}} V(\mathbf{k}, \mathbf{p}) G_0(\mathbf{k}, z) V(\mathbf{q} - \mathbf{k}, 2\mathbf{q} - \mathbf{p}) G_0(\mathbf{q}, z) \mathcal{V}(\mathbf{q}, \mathbf{p}, \lambda). \quad (\text{S11})$$

Here, one gets a similar result, as one can easily check.

3.+4.) The contributions from the A - and B -diagrams are of the wrong order, but the two terms cancel themselves in the hydrodynamic limit which gives the correct overall sound attenuation. Again, one has to focus on a single loop and disregard everything to the left. Note, that applying (S7) to the bare propagators in (4c) gives no significant contribution due to the identity $V(\mathbf{q}, 0) = 0$. So, the imaginary part arises from the terms containing the dressed propagator. For the resolvent one can use

$$\text{Im}G(\mathbf{q}, \lambda + i0^+) = \frac{\text{Im}\Sigma(\mathbf{q}, \lambda)}{\left(\lambda/n - \epsilon_0(\mathbf{q}) - \text{Re}\Sigma(\mathbf{q}, \lambda) \right)^2 + \text{Im}\Sigma(\mathbf{q}, \lambda + i0^+)^2} \xrightarrow{\lambda \rightarrow 0} -\pi \frac{n}{2c_T^2 q} \delta(\sqrt{\lambda/c_T^2} - q). \quad (\text{S12})$$

After performing the integral over \mathbf{q}, \mathbf{l} one can calculate the contribution from the third and fourth term of the vertex \mathcal{V} for vanishing \mathbf{p} . One gets

$$\begin{aligned} \text{Im}\mathcal{V}^{(3)}(\mathbf{k}, \mathbf{p}, \lambda + i0^+) &= \frac{1}{n} \sum_{\mathbf{l}} V(\mathbf{l}, \mathbf{k})^2 \text{Im}\left(G(\mathbf{l}, \lambda + i0^+)\right) G_0(\mathbf{k}, \lambda) \mathcal{V}(\mathbf{k}, \mathbf{p}, \lambda) \\ &\xrightarrow{\lambda \rightarrow 0} \frac{\pi S_3}{2(2\pi)^3 c_T^2} \left(\frac{\lambda}{c_T^2}\right)^{\frac{1}{2}} \epsilon_0(\mathbf{k}) \mathcal{V}(\mathbf{k}, \mathbf{p}, \lambda). \end{aligned} \quad (\text{S13})$$

One can use a similar line of argumentation to investigate the imaginary part of $\mathcal{V}^{(4)}$. The contribution in the small \mathbf{p} limit reads

$$\begin{aligned} \text{Im}\mathcal{V}^{(4)}(\mathbf{k}, \mathbf{p}, \lambda + i0^+) &= \frac{1}{n} \sum_{\mathbf{q}} V(-\mathbf{q}, \mathbf{k}) \text{Im}\left(G(\mathbf{q} + \mathbf{k}, \lambda + i0^+)\right) V(-\mathbf{k}, \mathbf{q}) G_0(\mathbf{q}, \lambda) \mathcal{V}(\mathbf{q}, \mathbf{p}, \lambda) \\ &\xrightarrow{\lambda \rightarrow 0} \frac{\pi S_3}{2(2\pi)^3 c_T^2} \left(\frac{\lambda}{c_T^2}\right)^{\frac{1}{2}} \epsilon_0(\mathbf{k}) \mathcal{V}(-\mathbf{k}, \mathbf{p}, \lambda). \end{aligned} \quad (\text{S14})$$

Adding both terms together yields

$$\text{Im}\left(\mathcal{V}^{(3)}(\mathbf{k}, \mathbf{p}, \lambda) + \mathcal{V}^{(4)}(\mathbf{k}, \mathbf{p}, \lambda)\right) \xrightarrow{\mathbf{p}, \lambda \rightarrow 0} \frac{\pi S_3}{2(2\pi)^3 c_T^2} \left(\frac{\lambda}{c_T^2}\right)^{\frac{1}{2}} \frac{\epsilon_0(\mathbf{k})}{n} \left(\mathcal{V}(\mathbf{k}, \mathbf{p}, \lambda) + \mathcal{V}(-\mathbf{k}, \mathbf{p}, \lambda)\right). \quad (\text{S15})$$

The important point is that the bracket vanishes in the hydrodynamic limit. This follows from the definition $V(\mathbf{q}, \mathbf{p}) = \hat{f}(\mathbf{q}) - \hat{f}(\mathbf{q} - \mathbf{p})$ and $\hat{f}(\mathbf{p}) = \hat{f}(-\mathbf{p})$ which holds due to rotational invariance. This gives

$$\begin{aligned} V(-\mathbf{k}, \mathbf{p} \rightarrow 0) &= \mathbf{p} \cdot \frac{\partial \hat{f}(\mathbf{k})}{\partial(-\mathbf{k})} = -V(\mathbf{k}, \mathbf{p} \rightarrow 0), \\ V(\mathbf{q}, \mathbf{k}) &= V(-\mathbf{q}, -\mathbf{k}). \end{aligned} \quad (\text{S16})$$

So, ignoring all initial momenta in the second, third and fourth term in \mathcal{V} and changing the integration variable $\mathbf{q} \rightarrow -\mathbf{q}$ gives in the small \mathbf{p} -limit for the vertex \mathcal{V} (4c)

$$\begin{aligned} \mathcal{V}(-\mathbf{k}, \mathbf{p}, z) &= -\frac{V(\mathbf{k}, \mathbf{p})}{n} + \frac{1}{n} \sum_{\mathbf{q}} \left(V(\mathbf{q} - \mathbf{k}, 2\mathbf{q}) + \sum_{\mathbf{l}} V(\mathbf{l}, \mathbf{q}) G(\mathbf{l}, z) V(\mathbf{l}, \mathbf{q}) \delta(\mathbf{k} - \mathbf{q}) \right. \\ &\quad \left. + V(-\mathbf{k}, \mathbf{q}) G(\mathbf{k} + \mathbf{q}, z) V(-\mathbf{q}, \mathbf{k}) \right) G_0(\mathbf{q}, z) \mathcal{V}(-\mathbf{q}, \mathbf{p}, z) = -\mathcal{V}(\mathbf{k}, \mathbf{p}, z). \end{aligned} \quad (\text{S17})$$

This holds since the only change the minus sign in the argument on the left-hand side inflicts on the right-hand side is in the final vertex $V(\mathbf{k}, \mathbf{p})$. But this vertex marks the end of any considered diagram. Hence, it appears exactly once in every occurring term. Thus, the imaginary contributions from $\mathcal{V}^{(3)}$ and $\mathcal{V}^{(4)}$ in (S15) cancel each other in the lowest order in \mathbf{p} . Consequently, the leading order must be $\lambda^{\frac{1}{2}} \mathbf{p}^4$ or $\lambda^{\frac{3}{2}} \mathbf{p}^2$, respectively.

In the main paper, we numerically calculate the imaginary part of the self energy around the sound pole $\lambda = \epsilon(\mathbf{p})$ in the two loop approximation. That is, truncating the equation for the renormalised vertex (4c) by replacing \mathcal{V} on the right hand side with the non-renormalised vertex V and setting $G \equiv G_0$ in the A - and B - blocks. The resulting diagrams are the ones from the second order perturbation theory. Since the used building blocks (S5) topologically coincides with the blocks of the second order perturbation theory, this numerical solution already implies that our full model predicts the correct sound attenuation. The analytical proof confirms this formally.

IV. ANALYTICAL RESULT FOR THE VIBRATIONAL DENSITY OF STATES

In this section, we analytically investigate the vDOS predicted by our model. The density of states in the eigenvalue domain is given by

$$g_\lambda(\lambda) = \frac{1}{N} \sum_{n=1}^N \delta(\lambda - \lambda_n) = -\frac{1}{N\pi} \text{Im} \sum_{i=1}^N \overline{\left[\frac{1}{\lambda + i0^+ - \mathbf{M}} \right]_{ii}}. \quad (\text{S18})$$

The trace of the resolvent is thus related to the high momentum limit of the propagator. The self-consistent equation for the high momentum limit read

$$\begin{aligned} G_\infty(z) &\equiv G(\infty, z) = [z/n - \hat{f}(0) - \Sigma(\infty, z)]^{-1} \\ \Sigma(\infty, z) &= \sum_{\mathbf{k}} \hat{f}(\mathbf{k}) \left[\mathcal{V}(\mathbf{k}, \infty, z) - \mathcal{V}'(\mathbf{k}, \infty, z) \right], \end{aligned} \quad (\text{S19})$$

with $\mathcal{V}'(\mathbf{k}, \infty, z) = \mathcal{V}(\mathbf{k} \rightarrow \mathbf{p} + \mathbf{k}, \mathbf{p} = \infty, z)$. The two renormalized vertices obey

$$\begin{aligned} \left(nG_0^{-1}(\mathbf{k}, z) - \underbrace{\sum_{\mathbf{q}} V^2(\mathbf{q}, \mathbf{k}) G(\mathbf{q}, z)}_A \right) \mathcal{V}(\mathbf{k}, \infty, z) &= \hat{f}(\mathbf{k}) + \sum_{\mathbf{q}} \left\{ \underbrace{\hat{f}(\mathbf{q} - \mathbf{k})}_{C} \mathcal{V}(\mathbf{q}, \infty, z) \right. \\ &\quad \left. - \left[\underbrace{\hat{f}(\mathbf{q} + \mathbf{k})}_C + \underbrace{V(-\mathbf{q}, \mathbf{k}) G(\mathbf{k} + \mathbf{q}, z) \hat{f}(\mathbf{k} + \mathbf{q})}_B \right] \mathcal{V}'(\mathbf{q}, \infty, z) \right\} \end{aligned} \quad (\text{S20})$$

and

$$\begin{aligned} \left(nG_0^{-1}(\infty, z) - \underbrace{\sum_{\mathbf{q}} \hat{f}(\mathbf{q})^2 [G(\mathbf{q}, z) + G_\infty(z)]}_A \right) \mathcal{V}'(\mathbf{k}, \infty, z) &= -\hat{f}(\mathbf{k}) - \sum_{\mathbf{q}} \left\{ \left[\underbrace{\hat{f}(\mathbf{q} + \mathbf{k})}_C \right. \right. \\ &\quad \left. \left. + \underbrace{\hat{f}(\mathbf{k} + \mathbf{q}) G(\mathbf{q} + \mathbf{k}, z) V(-\mathbf{k}, \mathbf{q})}_B \right] \mathcal{V}(\mathbf{q}, \infty, z) + \left[\underbrace{\hat{f}(\mathbf{q} - \mathbf{k})}_C + \underbrace{\hat{f}(\mathbf{q}) G_\infty(z) \hat{f}(\mathbf{k})}_B \right] \mathcal{V}'(\mathbf{q}, \infty, z) \right\}. \end{aligned} \quad (\text{S21})$$

Here, the letters A, B, C represent the respective building block (S5) from which the term originates.

a. High frequency limit and semi-circle law The boson-peak occurs at the upper limit of the dressed dispersion relation. For large eigenvalues, one has $|G(\mathbf{k}, z)| \approx |n/z| \ll 1$ for $\epsilon(\mathbf{k}) \ll \epsilon(\infty)$. Thus, we ignore all contributions to the self energy $\Sigma(\infty, z)$ that depend on $G(\mathbf{k}, z)$ or $G_0(\mathbf{k}, z)$. Looking at the equations for the renormalised vertex (S21), one notices, that the A and B blocks contribute with the same coefficient $a = \frac{1}{n} \sum_{\mathbf{k}} \hat{f}(\mathbf{k})^2$ in the considered approximation, if one ignores the C -diagrams. For the considered Gaussian spring function holds $a = \frac{\hat{f}(\mathbf{0})}{\sqrt{8n}}$. This gives the following self consistent equation for the high frequency limit of the resolvent

$$G_\infty^{-1}(z) = G_0^{-1}(\infty, z) - \frac{1}{2} \sum_{m=1}^{\infty} (2a)^m G_0(\infty, z)^m G_\infty(z)^{m-1} - \Sigma_C(z), \quad (\text{S22})$$

where Σ_C represents all the terms that contain at least one C -block. The term 2^{m-1} is a combinatorial factor. Since the geometric sum converges for n being sufficiently large, we get

$$1 = 2G_0^{-1}(\infty, z)G_\infty(z) - \frac{1}{1 - 2aG_\infty(z)G_0(\infty, z)} - 2\Sigma_C(z)G_\infty(z) \quad (\text{S23})$$

For large n , we can approximate Σ_C by the first two elements of perturbation theory $\Sigma_C = \Sigma_C^1 + \Sigma_C^2 + \dots$

$$\Sigma_C^1(z) = \frac{G_0(\infty, z)^2}{n^2} \sum_{\mathbf{k}, \mathbf{q}} \hat{f}(\mathbf{k}) \hat{f}(\mathbf{k} - \mathbf{q}) \hat{f}(\mathbf{q}) \quad (\text{S24})$$

$$\Sigma_C^2(z) = \frac{G_0(\infty, z)^3}{n^3} \sum_{\mathbf{k}, \mathbf{q}, \mathbf{l}} \hat{f}(\mathbf{k}) \hat{f}(\mathbf{k} - \mathbf{q}) \hat{f}(\mathbf{q} - \mathbf{l}) \hat{f}(\mathbf{l}). \quad (\text{S25})$$

Since the dressed dispersion relation is smaller than the bare one, we set $G_0(\infty, z) \approx -1/\hat{f}(\mathbf{0})$. Note, that this assumption is essential for the convergence of the infinite sum. This gives the quadratic equation

$$1 + \left(\frac{a}{\hat{f}(\mathbf{0})} - G_0^{-1}(\infty, z) + \Sigma_C(\infty, z) \right) G_\infty(z) + 2aG_\infty(z)^2 \approx 0, \quad (\text{S26})$$

where we neglected higher terms in $\Sigma_C G(\infty)$. It has the solution

$$G_\infty(z) = \frac{G_0^{-1}(\infty, z) - b \pm \sqrt{(z/n - \hat{f}(0) - b)^2 - 8a}}{4a} \quad (\text{S27})$$

with $b = \Sigma_C + \frac{a}{\hat{f}(0)}$. This gives the semi-circle law for the distribution of eigenvalues centered around $\omega_{BP}^2/n = \hat{f}(0) + b$ and with a width $\sqrt{8a}$. The maximal height of the resulting peak in the vDOS is hence $g_{\omega, max} = \frac{\sqrt{2}\omega_{BP}}{\pi n \sqrt{a}} \propto n^0$. That the height of the peak only depends on the bare spring function is an artefact of the applied approximations. Additionally, the ignored terms lead to a shift of this distribution to smaller frequencies. For n sufficiently high, one can approximate the dispersion relation with the bare dispersion. This gives for the relation of maximal height of the peak and the Debye level $\frac{g_{\omega, max}}{\omega_D^3} \propto n^{-\frac{5}{2}}$ for sufficiently high densities.

b. Low frequency limit and Debye law Contrary to the high frequency limit, for $z \rightarrow 0$, we can approximate $|G(\infty, z)| \approx 1/\hat{f}(0) \ll 1$. Setting terms equal to zero that contain at least one factor $G_0(\infty, z)$ highly simplifies the equations for the renormalised vertex. The amplitude of the remaining diagrams is given by

$$\Sigma(\infty, z) = \sum_{\mathbf{k}} \hat{f}(\mathbf{k}) \mathcal{V}(\mathbf{k}, \infty, z), \quad (\text{S28})$$

$$\mathcal{V}(\mathbf{k}, \infty, z) = \frac{\hat{f}(\mathbf{k}) + \sum_{\mathbf{q}} \hat{f}(\mathbf{k} - \mathbf{q}) \mathcal{V}(\mathbf{q}, \infty, z)}{n G_0^{-1}(\mathbf{k}, z) - \sum_{\mathbf{q}} V(\mathbf{q}, \mathbf{k})^2 G(\mathbf{q}, z)}. \quad (\text{S29})$$

Note, that the B -blocks are only implicitly present via the dressed propagator $G(\mathbf{q}, z)$. Since high momentum contributions of $G(\mathbf{q}, z)$ to the denominator are exponentially suppressed, one can approximate G with the hydrodynamic limit of the resolvent $nG^{-1} \approx z - \epsilon(\mathbf{q}) + i\omega(\mathbf{q})^3 q^2 \frac{B_R}{c_T^2}$. Here, we also added the two leading contributions to the damping together $\omega^3 q^2 B_R/c_T^2 \approx \omega^3 q^2 B_1 + \omega q^4 B_2$ which holds close to the sound pole $z \approx \epsilon(\mathbf{q})$, which in turn dominates the occurring integrals. For $\omega \rightarrow 0$ this leads to

$$\Sigma(\infty, z) = \sum_{\mathbf{k}} \hat{f}(\mathbf{k}) \mathcal{V}(\mathbf{k}, \infty, z), \quad (\text{S30})$$

$$\mathcal{V}(\mathbf{k}, \infty, z) \approx \frac{1}{n} \frac{\hat{f}(\mathbf{k}) + \sum_{\mathbf{q}} \hat{f}(\mathbf{k} - \mathbf{q}) \mathcal{V}(\mathbf{q}, \infty, z)}{G_0^{-1}(\mathbf{k}, z) - \sum_{\mathbf{q}} \frac{V^2(\mathbf{q}, \mathbf{k})}{z - \epsilon(\mathbf{q})} + i\omega^3 \frac{B_R}{c_T^2} h(\mathbf{k})}, \quad (\text{S31})$$

with $h(\mathbf{k}) = \sum_{\mathbf{q}} q^2 \frac{V^2(\mathbf{q}, \mathbf{k})}{\epsilon(\mathbf{q})^2}$. Considering the imaginary part of the self energy one obtains a term linear in ω . It originates from the sound pole in the denominator. Additionally, one gets a second term proportional to ω^3 . This term has a prefactor composed of a coefficient linear in B_R plus an off-set, which is independent of damping and results from the sound pole. While the first term leads to the Debye spectrum, the second term leads to the $g_{loc} = A_4 \omega^4$ vDOS of the quasi-localised modes for small frequencies.

One can write down the coefficient A_4 of the vDOS of QLMs. But first, we need to calculate $\text{Im}_{\omega^3} \Sigma$, which is the part of the imaginary part of the self energy that is proportional to $\omega^3 B_R/c_T^2$. We truncate the resulting series for $\text{Im}_{\omega^3} \Sigma$ after the first two contributions, but one can easily include more terms. One gets for $z \rightarrow 0$

$$\text{Im}_{\omega^3} \Sigma = \sum_{\mathbf{k}} \frac{\hat{f}(\mathbf{k})^2 h(\mathbf{k})/n}{\left(\hat{f}(0) - \hat{f}(\mathbf{k}) - \sum_{\mathbf{q}} \frac{V^2(\mathbf{q}, \mathbf{k})}{z - \epsilon(\mathbf{q})}\right)^2} + \sum_{\mathbf{k}, \mathbf{q}} \frac{2\hat{f}(\mathbf{k})h(\mathbf{k})/n^2}{\left(\hat{f}(0) - \hat{f}(\mathbf{k}) - \sum_{\mathbf{q}} \frac{V^2(\mathbf{q}, \mathbf{k})}{\epsilon(\mathbf{q})}\right)^2} \frac{\hat{f}(\mathbf{k} - \mathbf{q})\hat{f}(\mathbf{q})}{\hat{f}(0) - \hat{f}(\mathbf{q}) - \sum_{\mathbf{l}} \frac{V^2(\mathbf{l}, \mathbf{q})}{z - \epsilon(\mathbf{l})}} + \dots, \quad (\text{S32})$$

Here, the factor 2 is of combinatorial nature and results from the choice of which denominator one takes the imaginary part of. Note, that one can not approximate $\omega \approx 0$ in the equation above, since this would remove the sound pole, which contributes to the Debye spectrum. All in all, this gives

$$A_4 = n \frac{2 \text{Im}_{\omega^3} \Sigma}{\pi \epsilon(\infty)^2} \frac{B_R}{c_T^2}. \quad (\text{S33})$$

The leading order goes with $\propto n^{-5.5}$. In the main text, we compare (S33) with the simulation finding $\frac{c_T^4 \omega_{BP}^2}{B_R} A_4 \approx 0.01/2$ and the HET-prediction $A_4 = \frac{4}{2} \frac{B_R}{\pi \omega_{BP}^4 c_T^4} \frac{\omega_{BP}^2}{\omega_D^2}$ [8, 10, 14]. The additional factor 1/2 arises since we consider

only one transversal model. We find $c_T^4 \omega_{BP}^2 A_4/B_R \approx 0.045$ for $n = 0.5$ and thus reasonable agreement with the computational prediction. To compare to the HET-prediction, we set $\frac{\omega_{BP}^2}{\omega_D^2} \approx \frac{1}{36}$ as it has been found in [14]. Our predictions exceeds the HET-prediction by approximately a factor of ≈ 2.5

V. COMPARISON WITH THE PLANAR THEORY

The planar theory of the ERM model presented in [2, 39] is easily obtained from our self-consistent theory (4) by neglecting all the non-planar contributions of the B - and C -blocks. This leads to the following expression for the self energy [36]

$$\Sigma_P(\mathbf{p}, z) = \frac{1}{n} \sum_{\mathbf{k}} V^2(\mathbf{k}, \mathbf{p}) G(\mathbf{k}, z) = \sum_{\mathbf{k}} \frac{V^2(\mathbf{k}, \mathbf{p})}{z - n\epsilon_0(\mathbf{k}) - \sum_{\mathbf{q}} V^2(\mathbf{q}, \mathbf{k}) G(\mathbf{q}, z)}. \quad (\text{S34})$$

This straightforward re-summation can not capture all the salient features of disordered materials. As shown by Refs. [31, 39] and others, see section III, the planar theory predicts hydrodynamic damping instead of Rayleigh-damping. One can quickly show this by restating the argument from [39]: For $\mathbf{p} \rightarrow 0$, the main contribution to the self-energy arises from $k \gg p$. This gives

$$\text{Im}\Sigma_P(\mathbf{p}, z) = \frac{1}{n} \sum_{\mathbf{k}} V^2(\mathbf{k}, \mathbf{p}) \text{Im}G(\mathbf{k}, z) \approx \frac{1}{n} \text{Im}G(\infty, z) \sum_{\mathbf{k}} V^2(\mathbf{k}, \mathbf{p}) = -\pi g_\lambda(\lambda) \sum_{\mathbf{k}} V^2(\mathbf{k}, \mathbf{p}) \xrightarrow{\lambda, \mathbf{p} \rightarrow 0} -\frac{B_H}{n} \sqrt{\lambda} p^2. \quad (\text{S35})$$

Via $\text{Im}\Sigma_P(\mathbf{p}, z) \xrightarrow{\lambda, \mathbf{p} \rightarrow 0} -\frac{B_H}{n} \sqrt{\lambda} p^2$, we find the hydrodynamic damping coefficient. In figure 2, we compare the sound attenuation of the planar theory to the second order perturbation theory; for larger wavevector both lie close.

The absence of Rayleigh-damping also implies that the strength of the sound attenuation contributes linearly to the Debye-term of the vDOS instead of to the ω^4 -term. To see this, as [2]

$$\frac{1}{G_\infty(z)} = \frac{z - \epsilon_P(\infty, z)}{n} - a G_\infty(z) - \frac{1}{n} \sum_{\mathbf{k}} f^2(\mathbf{k}) \text{Im}G(\mathbf{k}, z), \quad (\text{S36})$$

with $a = \sum_{\mathbf{k}} / n$ as before, and $\epsilon_P(\mathbf{p}, z) = n(\epsilon_0(\mathbf{p}) - \text{Re}\Sigma(\mathbf{p}, z))$ being the renormalized dispersion relation of the planar theory. In the hydrodynamic limit ($\omega \rightarrow 0$), this gives the quadratic equation

$$1 = \left[\frac{z - \epsilon_P(\infty)}{n} + i\omega B_H \sum_{\mathbf{k}} k^2 \frac{f^2(\mathbf{k})}{\epsilon_p(\mathbf{k})^2} + i \frac{\omega f^2(\omega/c)}{4\pi c^3} \right] G_\infty(z) - a G_\infty(z)^2 + \mathcal{O}(B_H^2). \quad (\text{S37})$$

Here $\epsilon_P(\mathbf{p}) = \epsilon_P(\mathbf{p}, z = 0)$ and $c^2 = \lim_{\mathbf{p} \rightarrow 0} \frac{\epsilon_P(\mathbf{p})}{p^2}$ being the speed of sound of the planar theory. Note, that in [2] the authors approximated $G(\mathbf{k}, z) \approx G_0(\mathbf{k}, z)$ in equation (S36), thus the term linear in B_H is absent. For $n \rightarrow \infty$, one re-obtains their expressions since $\epsilon_P \propto n$ holds. For the density being sufficiently large, one gets

$$G_\infty(\lambda) \approx \left(\frac{\lambda - \epsilon_P(\infty)}{n} + i\omega B_H \sum_{\mathbf{k}} k^2 \frac{f^2(\mathbf{k})}{\epsilon_p(\mathbf{k})^2} + i \frac{\omega f^2(\omega/c)}{4\pi c^3} \right)^{-1} \quad (\text{S38})$$

It is noteworthy, that this expressions agrees with the one we would obtain, if we applied the low frequency approximation as in Sect. IV to the planar theory. One gets the Debye-level

$$n \frac{g_D(\omega)}{\omega^2} = \frac{2n^2 B_H}{\pi \epsilon(\infty)^2} \sum_{\mathbf{k}} k^2 \frac{f^2(\mathbf{k})}{\epsilon_p(\mathbf{k})^2} + \frac{n^2 \hat{f}(0)}{2\pi^2 \epsilon(\infty)^2 c^3} \quad (\text{S39})$$

Consequently, the Debye spectrum increases with an increasing sound attenuation coefficient. We interpret this as the absence of quasi-localised modes.

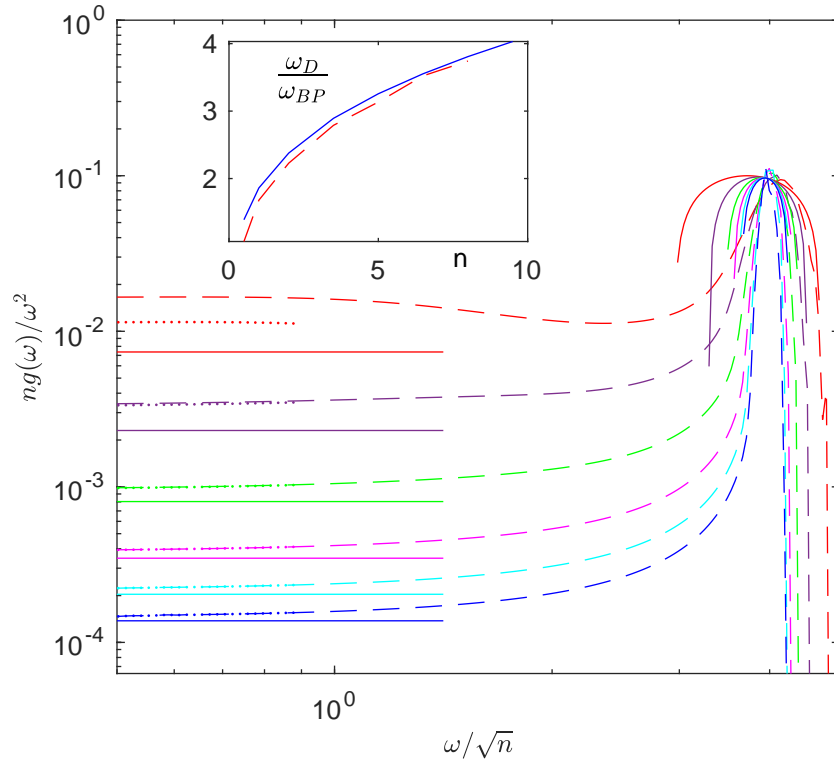


Figure S1. Comparison of the vDOS from Eq. (4) (full lines) with the prediction of the planar theory (dashed lines) for different n (see legend in Fig. 1). The dotted lines correspond to the Debye-level of the planar theory, Eq. (S39). The inset shows the associated ratio of Debye- over boson peak frequency. Here, the red dashed line shows the associated value of the planar theory. The blue solid line is the prediction of our model.

Lastly, in [2, 39], the boson peak was conceptualised as an excess over the Debye-vDOS which arises from an instability. Since the ERM-Model (Eq. 2) exhibits no such instability for a purely repulsive interaction, this instability is clearly an artifact of the approximations, as the authors of Ref. [2, 39] were aware. Since recent simulations suggest [14], that the boson peak does not only occur in marginally stable systems, we identified the boson peak with the occurring semi-circle. We emphasise that this excess over the Debye-law is still disorder-induced, since the characteristic frequency of the boson peak ω_{BP} is well below the Debye frequency ω_D . For stable glass states, we compare the vDOS of the planar theory to our results in Fig. S1.

VI. REFERENCES

For the list of references see the main paper.